Liquid-crystalline behavior of rod-coil diblock copolymers

M. W. Matsen[a] and C. Barrett
Polymer Science Centre, University of Reading, Whiteknights, Reading RG6 6AF, United Kingdom

(Received 27 March 1998; accepted 8 June 1998)

The exact mean-field phase behavior of the Semenov–Vasilenko model for rod-coil diblock copolymers is studied by applying self-consistent field techniques. The behavior depends on three quantities: the rod/coil immiscibility χN, the coil volume fraction f, and the ratio ν of the characteristic coil to rod dimensions. When $\chi N \lesssim 5$, the rods and coils mix producing a nematic phase, and at larger χN, they microphase separate forming a lamellar phase. The nonlamellar phases expected at $f \gtrsim 0.7$ are not treated here. The lamellar phase is typically a smectic-C structure with monolayers of tilted rods. A thorough understanding of the model is achieved by closely examining segment distributions and various contributions to the free energy. The tilt angle θ is generally controlled by a competition between rod/coil interfacial tension and stretching of the coils. Lowering f reduces the latter contribution, causing $\theta \to 0$ and producing a continuous transition to a smectic-A structure. Beyond that, there is a tendency to form structures with the rods arranged in bilayers, but this is strongly suppressed by a large steric penalty. We suggest that small amounts of solvent can greatly alleviate this penalty, and therefore could significantly affect some aspects of the phase behavior. © *1998 American Institute of Physics.* [S0021-9606(98)51534-6]

I. INTRODUCTION

Block copolymers are arguably the most ideal class of molecules for examining phenomena related to molecular self-assembly.[1] This is well demonstrated by the progress achieved in understanding the behavior of the classical coil-coil diblock copolymer. The highly analogous behavior of conventional lyotropic liquid crystals is still far from well understood even after many decades of study,[2] whereas, in contrast, we have developed detailed explanations for the polymeric system[3] over a relatively short period of time. This has been aided by a number of factors. The macromolecular nature of polymers is responsible for suppressing effects related to the atomic details, providing a system where the behavior is more universal and dependent on far fewer parameters. Furthermore, the macromolecular character suppresses fluctuation effects,[4] which tend to obscure the underlying mechanisms responsible for self-assembly. All this contributes to one further advantage, that being the ease with which polymeric systems can be accurately modeled.[5]

Another attractive feature of polymeric systems is the wide range of chemical monomers and sophisticated anionic synthesis techniques allowing scientists to tailor remarkably complex molecules. This versatility permits us to carefully examine a diverse range of phenomena. For instance, researchers can incorporate rigid blocks into these polymers in order to examine behavior characteristic of conventional thermotropic liquid crystals.[6] Just as with flexible block copolymers, the choice of possible architectures is endless, but it is natural to first consider the simplest, a rod-coil diblock, created by joining the end of a rigid rod to that of a flexible coil. The new feature of this block copolymer is its nontrivial steric interactions. Although the configurations of the flexible chain are highly restricted by its environment, the entropy loss is related to the ''free volume'' which remains more or less constant, and therefore its steric interactions can be ignored. On the other hand, the number of configurations accessible to the rigid block depends strongly on the shape of the ''free volume,'' which in turn depends on the orientation of the neighboring rods, and consequently the steric effects cannot be overlooked.

Previous work by Semenov and Vasilenko[7] introduced a well-suited microscopic model for rod-coil diblock copolymers, which accounts for the steric interactions among the rods, the stretching of the coils, and the unfavorable rod/coil interactions. The main innovation of their model is the effective way it accurately treats the steric effects. Although steric interactions are rather complicated, their net effect is simple; they cause the rods to select a preferred orientation, $\hat{\mathbf{n}}$, called the director. When the rods are long and concentrated, their orientation will fluctuate only slightly from the director, and to a good approximation these fluctuations can be ignored. Note that even with the rod orientation constrained to the $\hat{\mathbf{n}}$ direction, it is necessary to account for residual steric effects that prevent the rods from overlapping, but that is straightforward.[7] Although this treatment will break down at large coil volume fractions f, it should be accurate for most of the parameter space.

The original study by Semenov and Vasilenko[7] only considered the nematic phase and the smectic-A lamellar phases where the rods remain perpendicular to the lamellae. They did, however, allow the rods of the smectic phase to adopt either a monolayer or a bilayer configuration. Following that, Semenov[8] extended the calculation to include the smectic-C phases, where the rods could tilt by an angle θ to the lamellar normal (see Fig. 1). Shortly thereafter, Williams and Fredrickson[9] further extended the calculation to include

[a]Author to whom correspondence should be addressed.

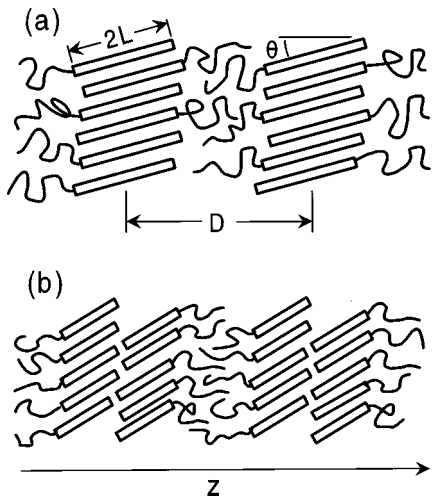

FIG. 1. Schematic illustrations of (a) monolayer and (b) bilayer smectic-C phases. The length of each rod is $2L=(1-f)Nb$ and its angle to the lamellar normal is θ. The smectic-A phases correspond to $\theta=0$.

nonlamellar phases, where the rods form finite-sized disks or ''pucks'' covered in a layer of coils, which would presumably pack together into some three-dimensional superstructure. They predicted that such phases should exist at large coil fractions ($f\gtrsim 0.9$).

Recently, experimentalists have created rod-coil diblock copolymers capable of testing these theoretical predictions. In particular, Chen *et al.*[10,11] have synthesized five copolymers by joining a highly rigid polyhexyl-isocyanate (PHIC) block to a flexible polystyrene (PS) coil. As expected, their samples formed smectic lamellar phases, but there were some interesting features not anticipated by the theory. In three of the samples, the lamellar order was very short range: one possessed ''wavy'' lamellar domains while the other two exhibited sharp ''zig-zag'' patterns. In contrast, the other two samples exhibited extraordinary long-range lamellar order over distances of up to almost a micrometer. Furthermore, these latter samples displayed an unusual smectic-O character, where the rod orientation flipped between successive layers. Radzilowski *et al.*[12] have synthesized rod-coil diblocks with larger coil fractions f, and have observed nonlamellar structures. Evidently, the lamellar rod domains transform to cylinders or ''strips'' near $f\sim 0.7$ and then to micellar aggregates or ''pucks'' near $f\sim 0.8$.

In this paper, we examine the Semenov–Vasilenko model much more accurately than the earlier studies. The previous efforts,[7–9] which were all based on mean-field theory, invoked a wide range of approximations to obtain analytic results in various limits. By piecing together those results a reasonably complete picture of the behavior was generated. However, these approximations are not necessary. Using self-consistent field techniques, we now examine the Semenov–Vasilenko model exactly within mean-field theory. For the moment, we have ignored the nonlamellar morphologies, and so our calculations are only valid for $f\lesssim 0.7$. Our results provide a few qualitative changes to the previously predicted phase diagram, but more importantly they provide quantitatively accurate predictions for comparison with future experiments. Our theoretical predictions do coincide reasonably well with previous experiments,[10,11] but we suggest there are some significant nonequilibrium effects that they need to address.

II. THEORY

In this section, we formulate the self-consistent field theory (SCFT)[5,13,14] for a system of n rod-coil diblock copolymers using the Semenov–Vasilenko model.[7] The segments are assumed to be incompressible and are defined based on a common volume, ρ_0^{-1}. The coil and rod blocks consist of fN and $(1-f)N$ segments, respectively, and therefore the total volume of the system is $\mathscr{V}=nN/\rho_0$. The coil segments are assumed to be completely flexible with a statistical length, a, and rod segments are completely rigid with a contour length, b. As mentioned in Sec. I, the model assumes that the steric interactions orient all the rods parallel to a common unit vector, $\hat{\mathbf{n}}$, which we call the director.

To specify the configuration of the αth molecule, we parametrize the flexible segments with a parameter, s, that varies from 0 at the free end to f at the junction. Then the function, $\mathbf{r}_\alpha(s)$, is defined as the contour of the coil, and $I_\alpha\in\{-1,1\}$ denotes whether the rod is oriented in the negative or positive $\hat{\mathbf{n}}$ direction. In terms of these quantities, the density of the flexible segments is

$$\hat{\phi}_C(\mathbf{r})=\frac{N}{\rho_0}\sum_{\alpha=1}^{n}\int_0^f ds\ \delta(\mathbf{r}-\mathbf{r}_\alpha(s)), \tag{1}$$

and the density of the rigid segments is

$$\hat{\phi}_R(\mathbf{r})=\frac{1-f}{2L}\int_{-L}^{L} dt\ \hat{p}_R(\mathbf{r}+t\hat{\mathbf{n}}), \tag{2}$$

where $L=(1-f)bN/2$ is half the rod length and

$$\hat{p}_R(\mathbf{r})=\frac{1}{n}\sum_{\alpha=1}^{n}\delta(\mathbf{r}-\mathbf{r}_\alpha(f)-I_\alpha L\hat{\mathbf{n}}) \tag{3}$$

is the midpoint distribution of the rods.

The Semenov–Vasilenko model uses the standard interaction energy,

$$\frac{\hat{U}}{k_BT}=\chi\rho_0\int d\mathbf{r}\ \hat{\phi}_C(\mathbf{r})\hat{\phi}_R(\mathbf{r}), \tag{4}$$

where χ is the Flory–Huggins interaction parameter. In general, the statistical mechanics of a large system of interacting molecules is intractable. To overcome this difficulty, we implement SCFT, where the interactions experienced by each molecule are represented by two static fields, $w(z)$ and $u(z)$, acting on $\hat{\phi}_C(\mathbf{r})$ and $\hat{p}_R(\mathbf{r})$, respectively. Recall that our study is limited to one-dimensional structures and so the fields only vary in the z direction (see Fig. 1).

The free energy functional for the Semenov–Vasilenko model is given by

$$\begin{aligned}\frac{F}{nk_BT}\equiv&-\ln(\mathscr{Q}/\mathscr{L})+\mathscr{L}^{-1}\int dz[\chi N\phi_C(z)\phi_R(z)\\&-w(z)\phi_C(z)-u(z)p_R(z)-\xi(z)(1-\phi_C(z)\\&-\phi_R(z))-p_R(z+L_z)\ln(1-\phi_R(z))],\end{aligned} \tag{5}$$

where $\mathscr{L}$ is the extent of the system in z direction, $\phi_C(z)$ is the thermodynamic average of $\hat{\phi}_C(\mathbf{r})$, $p_R(z)$ is the average of $\hat{p}_R(\mathbf{r})$,

$$\phi_R(z)=\frac{1-f}{2L_z}\int_{z-L_z}^{z+L_z}dz'\ p_R(z'), \tag{6}$$

$L_z=L\cos(\theta)$, and θ is the angle between $\hat{\mathbf{n}}$ and the z direction. The first term in Eq. (5) is the free energy of a molecule in the fields $w(z)$ and $u(z)$. It provides the appropriate entropy for the molecules, but its internal energy, which comes from the fields, has to be corrected. To do that, we add the interaction energy due to Eq. (4) and then subtract off the energy of the fields. The term with the Lagrange multipler, $\xi(z)$, is used to enforce the incompressibility condition, and the last term represents the entropy loss due to the steric interactions preventing the rods from overlapping.[7] The fields are determined by locating the extremum in F with respect to $\phi_C(z)$ and $p_R(z)$:

$$w(z)=\chi N\phi_R(z)+\xi(z), \tag{7}$$

$$u(z)=\frac{1-f}{2L_z}\int_{z-L_z}^{z+L_z}dz'\left[\chi N\phi_C(z')+\xi(z')+\frac{p_R(z'+L_z)}{1-\phi_R(z')}\right]-\ln(1-\phi_R(z-L_z)), \tag{8}$$

where $\xi(z)$ is determined by the constraint

$$\phi_C(z)+\phi_R(z)=1. \tag{9}$$

To proceed, we must solve the statistical mechanics of a single molecule in the fields, $w(z)$ and $u(z)$. Its partition function is given by

$$\mathscr{Q}\equiv\sum_{I_\alpha}\int\mathscr{D}\mathbf{r}_\alpha P[\mathbf{r}_\alpha;0,f]\times\exp\left\{-\int_0^f ds\ w(z_\alpha(s))-u(z_\alpha(f\ )+I_\alpha L_z)\right\}, \tag{10}$$

where $z_\alpha(s)$ represents the z component of $\mathbf{r}_\alpha(s)$. The weighting function,

$$P[\mathbf{r}_\alpha;s_1,s_2]=\exp\left\{-\frac{3}{2Na^2}\int_{s_1}^{s_2}ds\left|\frac{d}{ds}\mathbf{r}_\alpha(s)\right|^2\right\}, \tag{11}$$

accounts for the entropy loss of stretching the flexible coil. To make progress, we define

$$q(\mathbf{r},s)\equiv\int\mathscr{D}\mathbf{r}_\alpha P[\mathbf{r}_\alpha;0,s]\delta(\mathbf{r}-\mathbf{r}_\alpha(s))\times\exp\left\{-\int_0^s dt\ w(z_\alpha(t))\right\}, \tag{12}$$

which by symmetry depends only on the z coordinate, and which satisfies the modified diffusion equation,[13]

$$\frac{\partial}{\partial s}q(z,s)=\frac{1}{6}Na^2\frac{\partial^2}{\partial z^2}q(z,s)-w(z)q(z,s), \tag{13}$$

with the initial condition, $q(z,0)=1$. Similarly, we introduce

$$q^\dagger(\mathbf{r},s)\equiv\sum_{I_\alpha}\int\mathscr{D}\mathbf{r}_\alpha P[\mathbf{r}_\alpha;s,f]\delta(\mathbf{r}-\mathbf{r}_\alpha(s))\times\exp\left\{-\int_s^f dt\ w(z_\alpha(t))-u(z_\alpha(f\ )+I_\alpha L_z)\right\}, \tag{14}$$

which satisfies

$$\frac{\partial}{\partial s}q^\dagger(z,s)=-\frac{1}{6}Na^2\frac{\partial^2}{\partial z^2}q^\dagger(z,s)+w(z)q^\dagger(z,s) \tag{15}$$

with $q^\dagger(z,f\ )=\exp\{-u(z+L_z)\}+\exp\{-u(z-L_z)\}$. In terms of these functions,

$$\frac{\mathscr{Q}}{\mathscr{L}}=\int dz\ q(z,s)q^\dagger(z,s), \tag{16}$$

which can be evaluated for any value of s between 0 and f. Furthermore, the necessary densities are

$$\phi_C(z)=-\frac{\mathscr{L}}{\mathscr{Q}}\frac{\mathscr{D}\mathscr{Q}}{\mathscr{D}w(z)}=\frac{\mathscr{L}}{\mathscr{Q}}\int_0^f ds\ q(z,s)q^\dagger(z,s), \tag{17}$$

$$p_R(z)=-\frac{\mathscr{L}}{\mathscr{Q}}\frac{\mathscr{D}\mathscr{Q}}{\mathscr{D}u(z)}=p_{R+}(z)+p_{R-}(z), \tag{18}$$

where

$$p_{R\pm}(z)=\frac{\mathscr{L}}{\mathscr{Q}}q(z\mp L_z,f\ )\exp\{-u(z)\}. \tag{19}$$

This completes the list of expressions required to perform a SCFT calculation for the rod-coil diblock system. Careful examination reveals that only three parameters, χN, f, and $\nu\equiv aN^{1/2}/bN$, affect the phase behavior. To determine the stable state for a given set of parameters, we start by making an initial guess for $D/aN^{1/2}$, θ, $w(z)$, and $u(z)$. Given that, the concentrations, $\phi_C(z)$, $\phi_R(z)$, and $p_R(z)$, are calculated using Eqs. (13) and (15)–(19). Next, $w(z)$ and $u(z)$ are adjusted by a quasi-Newton–Raphson method so as to satisfy Eqs. (7)–(9). At this point, the free energy is calculated using Eq. (5). The final step is to minimize F with respect to $D/aN^{1/2}$ and θ. This entire procedure can be performed in real space, but we find it far more effective to expand all spatially dependent quantities in Fourier series and to work with their Fourier coefficients.[14] In fact, it was possible for us to keep the numerical inaccuracy absolutely negligible (i.e., less than one part in 10^6) without ever exceeding 50 harmonics.

The phase diagram for the rod-coil diblock system is determined by just examining the free energy. However, to actually understand the phase behavior, it is worthwhile to examine other quantities, such as the various segment distributions, and to break the free energy up into physically relevant contributions: $F=U-TS_{\rm fl}-TS_{\rm id}-TS_{\rm st}$, where U is the average interaction energy, $S_{\rm fl}$ is the entropy of the flexible segments, $S_{\rm id}$ is the ideal entropy of the rods, and $S_{\rm st}$ is the entropy correction due to the steric interactions between the rods. The explicit expressions for these four contributions are

$$\frac{U}{nk_BT}=\chi N\mathscr{L}^{-1}\int dz\ \phi_C(z)\phi_R(z), \tag{20}$$

$$-\frac{S_{\rm fl}}{nk_B}=-\mathscr{L}^{-1}\int dz[\{p_{R+}(z-L_z)+p_{R-}(z+L_z)\}\ln q(z,f)+w(z)\phi_C(z)], \tag{21}$$

$$-\frac{S_{\rm id}}{nk_B}=\mathscr{L}^{-1}\int dz[p_{R+}(z)\ln p_{R+}(z)+p_{R-}(z)\ln p_{R-}(z)], \tag{22}$$

$$-\frac{S_{\rm st}}{nk_B}=-\mathscr{L}^{-1}\int dz\ p_R(z+L_z)\ln(1-\phi_R(z)). \tag{23}$$

The expression for U is a straightforward consequence of Eq. (4) for the rod/coil interaction energy. To obtain $S_{\rm fl}$, we take the free energy of a coil with one end fixed at z [i.e., $\ln q(z,f)$], average it over the distribution of junctions [i.e., $p_{R+}(z-L_z)+p_{R-}(z+L_z)$], and then subtract off the internal energy contribution from the field, $w(z)$. The equation for $S_{\rm id}$ is an ideal-gas expression related to the number of ways the rods can be arranged given their distributions. The correction to this due to the steric interactions, $S_{\rm st}$, is derived in Ref. 7.

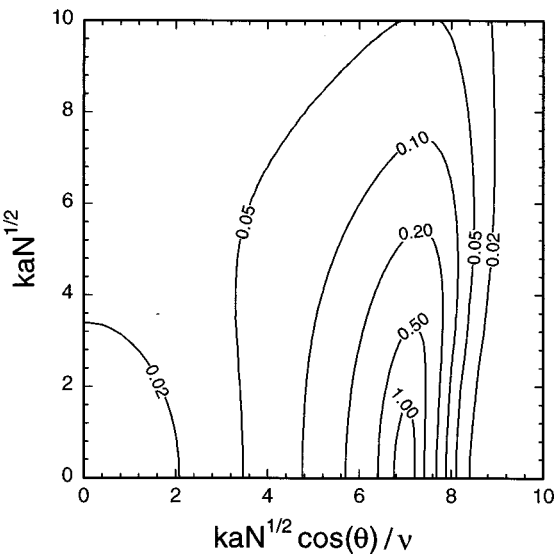

FIG. 2. Contour plot of the nematic-state structure function, $S_N(k,\theta)$, at $\chi N=6$ and $f=0.4$ plotted in terms of k and $k\cos(\theta)$, the magnitude and the $\hat{\mathbf{n}}$ component of the wave vector $\mathbf{k}$, respectively. For a given ν, only the region above the straight line of slope ν through the origin is physically relevant. In the small-ν limit, the scattering pattern can be considered as two disks orthogonal to $\hat{\mathbf{n}}$ a distance $\sim\pm 7\nu/aN^{1/2}$ along the $\hat{\mathbf{n}}$ axis each with a radius of $\sim 5/aN^{1/2}$. As ν increases, the disks shrink and begin to resemble simple pointlike peaks.

III. NEMATIC PHASE

We begin by considering the high-temperature nematic phase. In this phase, χN is too small to cause segregation of the rods and coils, and therefore the various distributions are uniform, i.e., $\phi_C(z)=f$, $\phi_R(z)=1-f$, and $p_{R\pm}(z)=1/2$. It is thus trivial to show that $U/nk_BT=\chi Nf(1-f)$, $-S_{\rm fl}/nk_B=0$, $-S_{\rm id}/nk_B=-\ln(2)$, and $-S_{\rm st}/nk_B=-\ln(f)$, from which it follows that the total free energy is $F_N/nk_BT=\chi Nf(1-f)-\ln(2f)$.

As the temperature is lowered, the nematic phase becomes unstable and transforms to a smectic phase. Within mean-field theory, the transition is generally continuous, and so it can be located by examining the free energy of a composition fluctuation, $\phi_C(\mathbf{r})\approx f+\phi_{C,1}\sqrt{2}\cos(\mathbf{k}\cdot\mathbf{r})$. To lowest order in the amplitude $\phi_{C,1}$, the free energy is

$$\frac{F}{nk_BT}\approx\frac{F_N}{nk_BT}+\frac{1}{2}S_N^{-1}(\mathbf{k})\phi_{C,1}^2, \tag{24}$$

where $S_N(\mathbf{k})$ is the nematic-state structure function. Because of the cylindrical symmetry about $\hat{\mathbf{n}}$, $S_N(\mathbf{k})$ depends only on the magnitude $k\equiv|\mathbf{k}|$ and the angle θ between $\mathbf{k}$ and $\hat{\mathbf{n}}$. In the Appendix, we show that

$$S_N^{-1}(k,\theta)=\frac{S_{11}+2S_{12}+S_{22}}{S_{11}S_{22}-S_{12}^2}+\frac{2\cos(kL_z)}{f\gamma}+\frac{1}{f^2}-2\chi N, \tag{25}$$

where

$$S_{11}=2(\exp(-xf)-1+xf)/x^2, \tag{26}$$

$$S_{12}=\cos(kL_z)\gamma(1-\exp(-xf))/x, \tag{27}$$

$$S_{22}=\gamma^2, \tag{28}$$

$$\gamma=(1-f)\sin(kL_z)/(kL_z), \tag{29}$$

$$x=k^2a^2N/6. \tag{30}$$

A large value of $S_N(k,\theta)$ indicates a small energetic penalty for a fluctuation of wave vector $\mathbf{k}$. When $S_N(k,\theta)$ diverges, the fluctuation becomes stable and the nematic phase transforms into a smectic phase.

Figure 2 shows a contour plot of the nematic-state structure function at $\chi N=6$ and $f=0.4$. So that we can consider all values of ν simultaneously, $S_N(k,\theta)$ is plotted as a function of $kaN^{1/2}$ and $kaN^{1/2}\cos(\theta)/\nu$. To interpret Fig. 2, it should be treated as a plot in terms of k and $k\cos(\theta)$, the magnitude of $\mathbf{k}$ and its component along the $\hat{\mathbf{n}}$ direction, respectively. Note that for finite values of ν, part of the plot is unphysical, specifically the portion below the straight line of slope ν through the origin.

In Fig. 2, $S_N(k,\theta)$ is finite everywhere, and so the nematic phase is stable for all values of ν at $\chi N=6$ and $f=0.4$. Notice, however, that there is region along $k\cos(\theta)\approx 7\nu/aN^{1/2}$, where the fluctuations are particularly strong. They become stronger as χN increases eventually producing a divergence when $\chi N=6.37$. The divergence occurs at $kaN^{1/2}=0$ and therefore only affects the $\nu=0$ limit, but as χN increases further, the divergence moves to larger $kaN^{1/2}$ affecting finite values of ν. Diblocks with $\nu=0.25$ experience the divergence at $\chi N=6.51$, which transforms them to a smectic-A ($\theta=0$) phase with a period, $D/aN^{1/2}=3.61$. In the case $\nu=0.5$, the transition occurs at $\chi N=7.11$ producing a smectic-A phase with $D/aN^{1/2}=1.76$. For $\nu=1.0$, the smectic-A phase does not occur until $\chi N=10.59$, and its period is only $D/aN^{1/2}=0.92$.

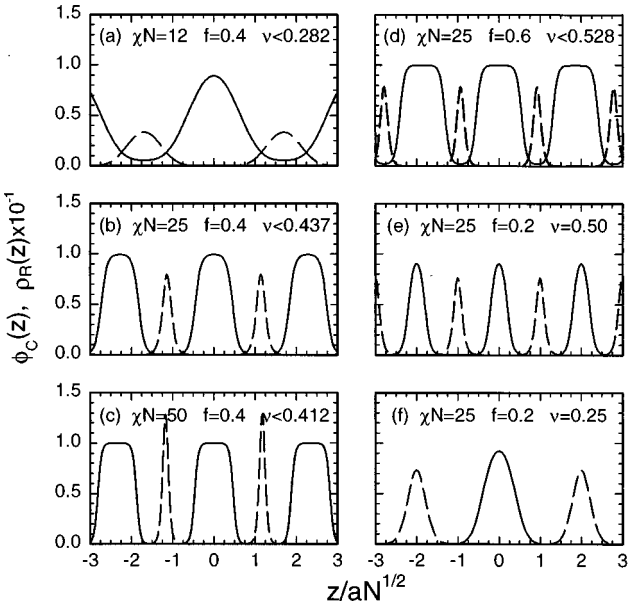

FIG. 3. Plots of $\phi_C(z)$ (solid curves) and $p_R(z)$ (dashed curves) for a selection of smectic monolayer phases. The first four, (a)–(d), correspond to smectic-C phases provided ν is less than the indicated values, and the last two, (e) and (f), are for smectic-A phases where a large ν prevents the rods from tilting.

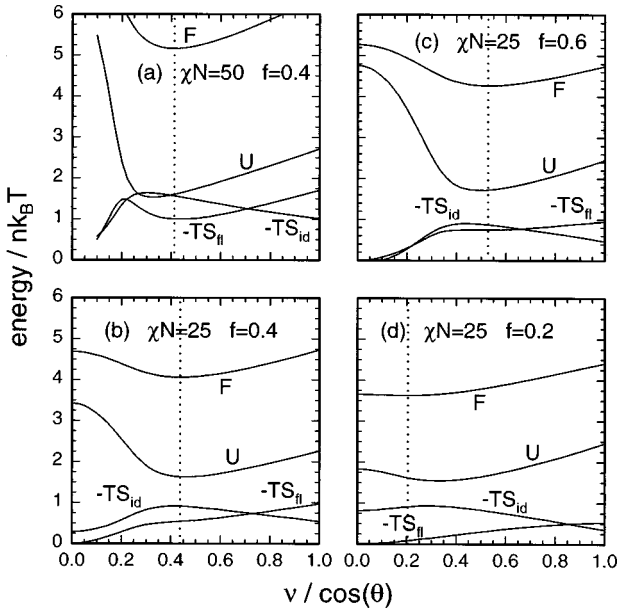

FIG. 4. Free energy F and three of its contributions, U, $-TS_{\rm fl}$, and $-TS_{\rm id}$, plotted as a function of tilt angle θ for the smectic monolayer phases. Recall that the $-TS_{\rm st}$ contribution is nearly constant [see Eq. (32)]. To a good approximation, the horizontal axis represents the lamellar period since $D/aN^{1/2}\approx \nu/\cos(\theta)$. The vertical dotted lines denote the equilibrium angle in the smectic-C phase, unless ν is too large in which case the most stable state is smectic-A with $\theta=0$.

In general, the nematic/smectic transition is relatively insensitive to ν until $\nu\sim 1$, where it starts to move rapidly toward large χN. To reveal this behavior move clearly, we examine the $f\to 0$ limit, where the divergence in $S_N(k,\theta)$ can be calculated analytically. In this limit, the transition occurs at

$$\chi N=\frac{\pi^2}{2}\left(1+\frac{\pi^2\nu^4}{9}\right), \tag{31}$$

where the smectic phase has a wave vector of $kaN^{1/2}=2\pi\nu$ and a tilt angle of $\theta=0$. Clearly, the ν^4 dependence in Eq. (31) accounts for the way the transition shifts with increasing ν.

IV. SMECTIC MONOLAYER PHASES

We now examine the smectic lamellar phases that form when χN becomes sufficient to cause segregation between the rods and coils. Just above the nematic/smectic transition, the rod layers are very broad, but as χN increases, the rods align forming well-defined monolayer domains as depicted in Fig. 1(a). At this point, the repeat period of the smectic phase is $D/aN^{1/2}\approx\cos(\theta)/\nu$, where θ is the tilt angle of the rods. If $\theta=0$, then the phase is called smectic-A, and if $\theta>0$, then it is smectic-C.

Much can be learned about the smectic phases by just examining how their segment distributions depend on χN, f, and ν. With this intent, Fig. 3 plots the coil segment distribution, $\phi_C(z)$, and the center of mass distribution of the rods, $\rho_R(z)$, for a representative selection of parameters. The sequence in Figs. 3(a)–3(c) illustrates how the smectic-C phase develops as χN increases with a fixed composition of $f=0.4$. At the weak segregation of $\chi N=12$, the profiles of the smectic-C phase are broad and poorly developed. Note that ν only affects the tilt angle, which is given by $\theta=\cos^{-1}(\nu/0.282)$; if ν happens to be larger than 0.282, then a smectic-A phase will occur instead. At $\chi N=25$, the profiles become reasonably developed and the tilt angle increases to $\theta=\cos^{-1}(\nu/0.437)$. At the strong segregation of $\chi N=50$, the tilt angle decreases to $\theta=\cos^{-1}(\nu/0.412)$ in order to reduce the interfacial area. The remaining three plots in Fig. 3 examine the intermediate degree of segregation at $\chi N=25$ as f is varied. Figure 3(d) shows that a rise in the coil composition to $f=0.6$ increases the tilt angle to $\theta=\cos^{-1}(\nu/0.528)$ so as to relax the highly stretched coils. Naturally, lowering the composition to $f=0.2$ has the opposite effect reducing the tilt angle to $\theta=\cos^{-1}(\nu/0.204)$, provided that $\nu<0.204$. If ν is larger, then a smectic-A phase results; Figures 3(d) and 3(e) show profiles for this particular situation.

Another way to enhance our understanding of the smectic phases is to examine the free energy F and its four contributions in Eqs. (20)–(23). As it turns out, the contribution from the steric interactions is fairly trivial. Assuming reasonably segregated monolayer rod domains and using Eq. (6) to obtain an approximate relation between $d\phi_R$ and dz, the steric energy in Eq. (23) becomes

$$-\frac{S_{\rm st}}{nk_B}\approx-\int_0^1 d\phi_R\,\ln(1-\phi_R)=1. \tag{32}$$

Consequently, the steric interactions play a rather minor role in the behavior of the monolayer phases, but this is not so for the bilayer phases discussed in Sec. V.

Figure 4 plots the three remaining free energy contributions as a function of $\nu/\cos(\theta)$, which is approximately the

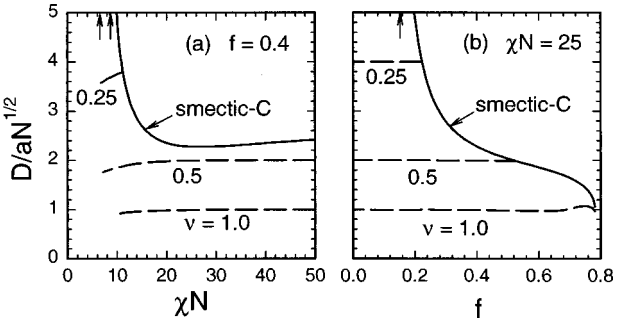

FIG. 5. Domain spacing D of the smectic lamellar phases plotted (a) as a function of χN at $f=0.4$ and (b) as a function of f at $\chi N=25$. If ν is not too large, the system will generally adopt the smectic-C monolayer phase with a spacing given by the solid curve. Otherwise, the smectic-A monolayer phase occurs with $D/aN^{1/2}\approx\nu^{-1}$ as indicated by the dashed curves. The $D\to\infty$ limits of the smectic-C curves are marked by arrows, and in (a) the nematic/smectic-A transition for $\nu=0$ is also denoted by an arrow.

inverse domain spacing, $(D/aN^{1/2})^{-1}$. It is most instructive to first focus on the strongly segregated case in Fig. 4(a). At large $\nu/\cos(\theta)$ (i.e., small $D/aN^{1/2}$), F is dominated by the interfacial energy[7] from U and $-TS_{\rm fl}$. Since this energy is proportional to the total interfacial area, F is roughly linear with $\nu/\cos(\theta)$. At smaller values of $\nu/\cos(\theta)$ (i.e., large $D/aN^{1/2}$), $-TS_{\rm fl}$ picks up an additional contribution from the coil stretching, which produces a minimum in F at $\nu/\cos(\theta)=0.412$. Provided that $\nu<0.412$, the system adopts this minimum and exhibits a smectic-C phase; otherwise, it comes as close as possible by forming a smectic-A phase with $\theta=0$. The behavior to the left of the minimum at small $\nu/\cos(\theta)$ seems a bit odd, but there is a simple explanation. As $\nu/\cos(\theta)$ approaches zero, the highly stretched coils start pulling rods into their domains, which allows them to relax but produces a wide rod/coil interface. This is reflected by a sharp rise in U and a dramatic drop in $-TS_{\rm fl}$ and $-TS_{\rm id}$. The resulting situation, which occurred in Figs. 3(e) and 3(f), is what Semenov and Vasilenko[7] call the ''neutral'' state. For the strongly segregated case in Fig. 4(a), the rise in U dominates the reduction in $-TS_{\rm fl}$ and $-TS_{\rm id}$, and so the neutral state is unstable. However, this changes as either χN or f is reduced. Notice that in Fig. 4(d), the minimum in F is much shallower and is shifted toward $\nu/\cos(\theta)=0$. At lower χN or f, the minimum disappears allowing a neutral smectic-A state to occur. Note that the crossover to the neutral state is not an actual phase transition.

To complete our understanding of the smectic monolayer phases, we now examine the domain spacing D as a function of χN and f in Figs. 5(a) and 5(b), respectively. In both plots, the solid curve represents the period associated with the free energy minima in Fig. 4. First, we consider the $\nu=0$ limit, where the smectic phase can achieve this desired period by selecting an appropriate tilt angle θ. In Fig. 5(a) where $f=0.4$, the nematic phase transforms to a neutral smectic-A phase at $\chi N=6.37$ and then to a smectic-C phase at $\chi N=8.61$. As χN increases, the population of rods extending deep into the coil domains drops, making it necessary for the coils to stretch in order to satisfy the incompressibility condition [i.e., $\phi_C(\mathbf{r})+\phi_R(\mathbf{r})=1$]. To alleviate some of the stretching, D decreases by tilting the rods. At the intermediate segregation $\chi N\approx 25$, the interfacial tension starts to take over and D begins to increase. In Fig. 5(b) where $\chi N=25$, the neutral smectic-A state occurs for $f<0.151$, where the rods are able to penetrate the thin coil domains. For larger f, the rods are expelled from the coil domains causing the coils to stretch. Of course, the stretching penalty is further amplified by the increase in coil size, and consequently there is a sizable reduction in D.

The maximum domain spacing in a smectic monolayer phase is approximately $aN^{1/2}/\nu$, and thus it is not always possible to achieve the desired domain spacing plotted in Fig. 5 with the solid curves. Roughly speaking, if ν^{-1} falls below the solid curves, a smectic-A phase will occur with $D/aN^{1/2}\approx\nu^{-1}$. The dashed curves show actual values of $D/aN^{1/2}$ for $\nu=0.25$, 0.5, and 1.0. Notice that at weak segregations near the nematic/smectic boundary, small χN in Fig. 5(a) or large f in Fig. 5(b), there is a significant deviation from $\cos(\theta)/\nu\approx D/aN^{1/2}$. Also note that there are various features evident in Fig. 5 such as nematic/smectic-A and smectic-A/smectic-C transitions, which will show up in our phase diagrams in Sec. VI.

V. SMECTIC BILAYER PHASES

As illustrated in Fig. 5(a), the large interfacial energy that occurs at high degrees of segregation forces the smectic-C phase to expand its period by reducing the tilt angle θ. Of course, once the monolayer phase becomes smectic-A (i.e., $\theta=0$), the system must find another way to lower its interfacial area. This can be done by transforming to a bilayer phase [see Fig. 1(b)], where the domain spacing is $D/aN^{1/2}\approx 2\cos(\theta)/\nu$. Although this can potentially reduce the interfacial area by a factor of 2, the steric penalties are greatly increased due to the restrictions placed on the rods. In the monolayer phase, the rods are free to slide independently, but in the bilayer phase, the rods are arranged end-to-end and thus they must move in pairs so as not to violate the incompressibility condition at the center of the rod domains.

Even at the strong segregation of $\chi N=50$, the steric penalty is generally far too great to permit a stable bilayer phase. The exception is at large ν, where the smectic-A monolayer phase can build up significant interfacial energy because of its small period, $D/aN^{1/2}\approx\nu^{-1}$. For $\nu=1.0$ and $\chi N=50$, a stable smectic-A bilayer phase occurs for $0.0957<f<0.3001$. One might expect a smectic-C bilayer phase to occur intermediate to the two smectic-A phases,[8] but it does not. Once the bilayer phase forms, the extreme interfacial energies required to overcome the steric penalty immediately force the tilt angle to zero. At much stronger degrees of segregation, there will exist conditions where the bilayer smectic-C phase becomes stable.[8]

Figure 6 compares the profiles, $\phi_C(z)$ and $p_R(z)$, of the monolayer and bilayer smectic-A phases on the phase boundary at $\chi N=50$ and $f=0.3001$. Due to the fixed composition, both the rod and coil domains are twice as thick in the bilayer phase as compared to the monolayer phase. It is important to notice that the bilayer phase has a sizable concentration of coil segments in the middle of each rod domain. As f decreases to 0.0957, this concentration increases con-

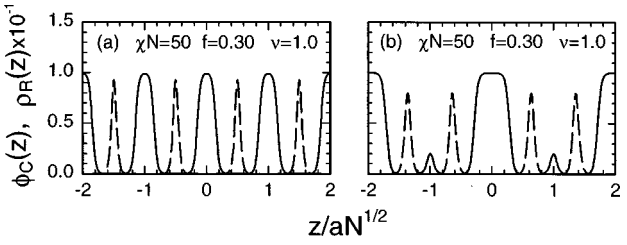

FIG. 6. Plots of $\phi_C(z)$ (solid curves) and $p_R(z)$ (dashed curves) for the smectic-A (a) monolayer and (b) bilayer phases along their phase boundary at $\chi N=50$, $f=0.3001$, and $\nu=1.0$.

tinuously, transforming the bilayer phase back into the monolayer phase.

To reveal the issues involved in selecting between the monolayer and bilayer phases, Fig. 7 compares their free energy contributions, Eqs. (20)–(23), as a function of f. Figure 7(a) shows the reduction in the interaction energy U as a result of switching to the bilayer structure. The reduction is substantial, but not a factor of 2 as it could be if the center of the rod domains were free of coils. The entropic energy of the coils, shown in Fig. 7(b), is more closely matched. Although the coils are far more stretched in the bilayer phase, this is countered by a reduction in the interfacial entropy loss,[7] causing $-TS_{\rm fl}$ to be slightly smaller in the bilayer phase. The entropic energy of the rods, $-TS_{\rm id}$, is lower in the monolayer phase because each rod can adopt either orientation, i.e., $I_\alpha=\pm 1$. As we have discussed above, there are large steric penalties in the bilayer phase and this is illustrated by Fig. 7(d). Although $-TS_{\rm st}$ is quite large for the bilayer phase, it would be much larger, if it were not for the small concentration of coils in the middle of the rod domain. Because the flexible coils can fill small gaps, where the rods meet at the center of the domain, they relieve a great deal of the steric penalty, but for a significant cost in U. A small amount of compressibility or a small concentration of an appropriate solvent are other less expensive alternatives that could dramatically stabilize the bilayer phase.

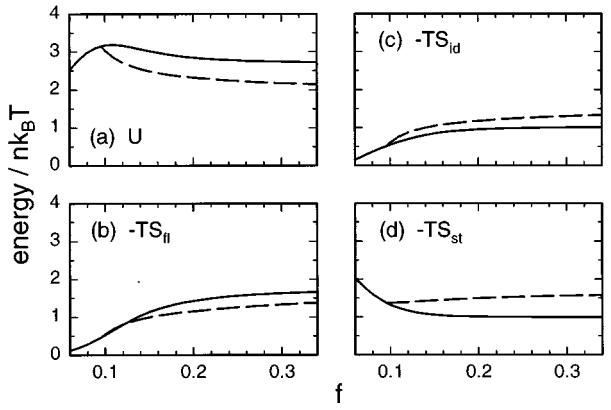

FIG. 7. Contributions to the free energy F as a function of composition f for $\chi N=50$ and $\nu=1.0$. The solid curves correspond to the smectic-A monolayer phase and the dashed curves represent the smectic-A bilayer phase. The bilayer phase is stable for $0.0957<f<0.3001$.

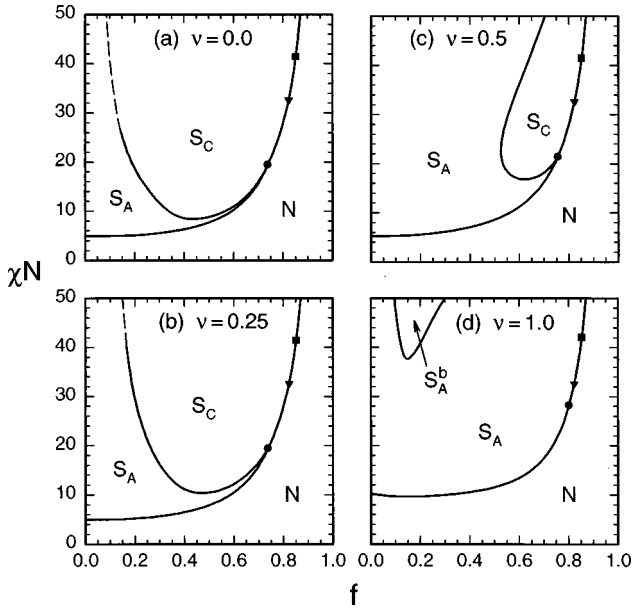

FIG. 8. Phase diagrams plotted in the χN-f plane for (a) $\nu=0.0$, (b) $\nu=0.25$, (c) $\nu=0.5$, and (d) $\nu=1.0$, denoting the stable regions for the nematic (N), monolayer smectic-A (S_A), bilayer smectic-A (S_A^b), and monolayer smectic-C (S_C) phases. The N/S boundaries are continuous to the left of each square, and the S_A/S_C boundaries are also continuous. The intersections of these boundaries are marked with circular dots. Note that in (d), the S_C phase exists but is too small to be resolved. The S_A^b phase in (d) is bounded on the left and right by continuous and discontinuous transitions, respectively. The dashed curves denote extrapolated boundaries, which could not be calculated due to numerical difficulties.

VI. PHASE DIAGRAM

Figure 8 presents the phase diagram showing specifically where the various nematic and smectic phases are stable. The phase diagram has three axes corresponding to χN, f, and ν, but instead of trying to construct a three-dimensional plot, we present a series of cuts though the diagram with ν fixed at 0.0, 0.25, 0.5, and 1.0. In each χN-f plane, we examine χN from 0 to 50 and f over the entire range, 0 to 1. There seems little point of examining the strong-segregation regime beyond $\chi N=50$, because nonequilibrium effects are certain to prevent experiments from accessing the behavior. At any rate, we have difficulty solving the self-consistent field equations once the rod domains become extremely pure; we use dashed lines for those boundaries which could not be evaluated. Although we examine the entire range of f, be aware that the nonlamellar phases expected for $f\gtrsim 0.7$ are not considered in our study. Typical rod-coil molecules correspond to values of $\nu\lesssim 0.25$ (see Table I), but for completeness and so that we can study a stable bilayer phase, larger values of ν are also considered.

As discussed in Sec. III, the phase boundary separating the high-temperature nematic phase from the low-temperature smectic phases is generally continuous within mean-field theory. Therefore, it can be located by determining when the nematic-state structure function, $S_N(k,\theta)$, in Eq. (25) develops a divergence. The wave vector of the divergence provides the domain spacing and tilt angle of the resulting smectic phase. For $f\lesssim 0.7$ or more specifically to the right of the dots in Fig. 8, the divergence in $S_N(k,\theta)$

occurs at $\theta=0$, and thus the nematic phase transforms into a smectic-A phase. Between the dots and the triangles, $S_N(k,\theta)$ diverges at $\theta>0$ producing a smectic-C phase, and between the triangles and the squares, $S_N(k,\theta)$ diverges at $\theta=90°$ producing an unusual phase that almost immediately transforms discontinuously to a regular smectic-C phase. This $\theta=90°$ phase exists in a region that is far too narrow to be resolved on the scale of Fig. 8. Beyond the squares, the nematic/smectic boundary is discontinuous. In reality, we should pay no attention to the phase behavior beyond $f\sim 0.7$, because it will be altered by the nonlamellar phases omitted in our study.

Emerging from the solid dots in Fig. 8 is the smectic-A/smectic-C transition. Note that a smectic-C region does exist in Fig. 8(d), but it is far too narrow to be resolved on that scale. The smectic-A/smectic-C boundary is continuous, apart from one absolutely negligible exception. When $\nu\approx 0$, there is an extremely short interval of length $\Delta f\sim 0.002$ next to the nematic phase where the smectic-A/smectic-C transition is weakly discontinuous.

In the $\nu=0$ limit, the entire smectic-A phase is neutral with completely relaxed coils. As ν increases, the smectic-A phase consumes a portion of the smectic-C phase. In this new region of smectic-A, the coils can become reasonably stretched. However, there is no actual phase transition distinguishing the relaxed- and stretched-coil regions of the smectic-A phase.[8]

When ν is large, the monolayer smectic-A phase develops a sufficiently high interfacial energy that it switches to a bilayer smectic-A phase as illustrated in Fig. 8(d). The bilayer (S_A^b) phase is bounded on the right by a discontinuous transition and on the left by a continuous one. The discontinuous transition occurs when the coils become sufficiently relaxed to allow the interfacial tension to overcome the steric penalty of forming bilayers. As the coil size is reduced further, the penalty for placing coils at the center of a rod domain monotonically drops, and consequently the concentration of coil segments in the rod domains rises eventually producing a continuous transition back to the monolayer phase.

VII. DISCUSSION

One of the challenges in extending the successes achieved in modeling flexible block copolymer molecules[3–5] to architectures involving rigid blocks is to accurately treat the steric interactions. A study by Müller and Schick[15] has clearly demonstrated that they cannot be ignored. When steric effects are omitted, a cylindrical morphology occurs where the lamellar structures should be.[15] In general, steric interactions are too complicated to treat by an accurate first-principles approach, but fortunately their net effect can be mimicked by constraining the rod orientation to a particular direction, $\hat{\mathbf{n}}$. If, as in the present case, the rods are long and highly concentrated, this approximation should be very accurate. However, as pointed out by Semenov and Vasilenko,[7] this constraint is not sufficient since the rods can still overlap, but this latter consideration can be taken into account by using the steric energy in Eq. (23). In many works,[16] steric effects have been treated by conventional Maier–Saupe two-body interactions. While this is more suitable for short rods, semiflexible blocks, and dilute rod concentrations, it is not appropriate for the rod-coil diblock copolymers examined in our study.

The steric interactions impart liquid-crystalline behavior upon the rod-coil diblock system causing the high-temperature phase to be nematic and the microphase separated structures to be smectic. If the segregation is weak or if the coil domains are narrow, a neutral smectic-A phase results, where the coils avoid stretching by pulling rods into their domains. However, when χN and f are large, this becomes costly and the rod/coil interface becomes narrow. At this point, the behavior is largely dictated by the stretching energy, which is proportional to fD^2, and by the interfacial energy, which is proportional to γ/D, where γ is the rod/coil interfacial tension. Packing constraints require $D\propto\cos(\theta)$, and thus the equilibrium tilt angle θ roughly obeys $\cos(\theta)\propto(\gamma/f)^{1/3}$. At large f or small χN, a monolayer smectic-C phase generally occurs with a high degree of tilt, and as f decreases or χN increases, $\theta\to 0$ eventually producing a continuous transition to a smectic-A phase. We note that Halperin[17] argued that the interfacial energy should be proportional to $\gamma(1+|\tan(\theta)|)$, which in this case would predict a strong discontinuous transition from $\theta=45°$ to $\theta=0°$. Semenov[8] has pointed out flaws in his argument. First Halperin assumes an ideal interface where the rods are tightly packed and perfectly aligned [i.e., $p_R(z)$ is represented by a series of Dirac delta functions]. Under this condition, the area of contact between the coils and the rods would depend sensitively on the detail shape of the rod ends, for which he made a rather artificial choice. Fortunately, in a realistic case, where $p_R(z)$ has some finite width producing a somewhat rough interface, the molecular detail will not be important and our treatment should be accurate.

Our calculation has ignored crystallization effects, which are common among rigid blocks. At high rod concentrations or low temperatures, the rods will typically crystallize quantizing the orientation θ to a small set of discrete values. This will split the smectic-C phase up into a series of regions, one for each of the allowed angles θ, separated by discontinuous phase transitions. Undoubtedly, these boundaries would be difficult if not impossible to experimentally locate, because of the severe nonequilibrium effects associated with the huge energy barriers involved in changing θ. Therefore, it would be highly desirable to work with rods which do not crystallize.

Once $\theta=0$, the smectic monolayer phase in Fig. 1(a) can only increase its domain spacing by switching to the bilayer arrangement in Fig. 1(b). In principle, we might expect a smectic-C bilayer phase to initially form followed by a continuous transition to a smectic-A bilayer phase. However, we found that the interfacial penalty required to overcome the steric penalty is so great that once the bilayer phase forms, θ immediately becomes zero. In fact, for intermediate degrees of segregation ($\chi N\lesssim 50$), the interfacial tension can only overcome the steric penalty of a bilayer phase when ν is unrealistically large, and once it forms, a significant concentration of coil segments accumulate at the center of the rod

TABLE I. Smectic phases of the rod-coil diblock copolymers in Ref. 11.

Sample	N[a]	f[b]	ν[c]	θ	Rod domain	Morphology
HS73/104	1360	0.58	0.11	60°	Monolayer	Wavy lamellar
HS63/14	390	0.27	0.20	45°	Bilayer	Zig-zag
HS58/7	510	0.10	0.17	45°	Bilayer	Zig-zag
HS245/9	2000	0.035	0.087	45°	Bilayer	Arrowhead
HS386/7	3090	0.017	0.070	45°	Monolayer	Arrowhead

[a]Defined using $\rho_0^{-1}=211$ Å^3, the estimated volume of a PHIC monomer.
[b]Calculated using PS and PHIC mass densities of 1.04 and 1.00 g/cm^3, respectively.
[c]Calculated using $a=7.57$ Å and $b=1.95$ Å.

domains [see Fig. 6(b)]. The small distribution of flexible coils is far better at filling space uniformly than the rigid rods, and thus they greatly reduce the steric penalty, justifying the costly rod/coil contacts. Alternative ways of reducing the high steric penalties are to include a finite compressibility or another component in the system. In particular, a selective solvent for the rods should be very effective.

When f is large, the lamellae are forced to break into small aggregates to allow the highly stretched coils to spread out and relax. Experiments by Radzilowski *et al.*[12] have shown that the rod lamellae first break into long ''strips'' at $f\sim 0.74$ and then into smaller micellelike ''pucks'' near $f\sim 0.8$. This progression is analogous to the situation in conventional coil-coil diblock copolymer systems, where the minority lamellae switch to cylinders and then to spheres as the majority block becomes larger. Williams and Fredrickson anticipated the pucklike aggregates for $f\gtrsim 0.88$ by extending the Semenov–Vasilenko calculation. However, they did not consider striplike aggregates, nor did they allow for smectic-C type structures where the rods are tilted.[6] Furthermore, their calculation used strong-segregation approximations, and it ignored the steric energy in Eq. (23), which is very important in bilayer structures. Now that the situation is better understood and there is an exact mean-field method for examining the model, it would be nice to reconsider the nonlamellar morphologies.

Although our mean-field calculation should, in general, be accurate for high molecular-weight molecules,[7] fluctuations will modify the nematic/smectic boundary. When mean-field theory predicts a continuous nematic to smectic-C transition, the structure function, $S_N(\mathbf{k})$, diverges on two circular rings oriented perpendicular to the director, $\hat{\mathbf{n}}$. Because the divergence is not isolated to points, Brazovskii fluctuations[18] will impart a discontinuity to the transition. As the tilt angle, θ, in the smectic-C phase approaches zero, the rings will shrink to points suppressing the Brazovskii fluctuations. Thus one would normally expect the nematic/smectic-A transition to remain continuous. However, an exception arises when $\nu\to 0$, because the two pointlike peaks in $S_N(\mathbf{k})$ broaden into two disks oriented perpendicular to $\hat{\mathbf{n}}$. The diameter of the disks, which is of order $1/aN^{1/2}$, can be much larger than their separation, which is of order $\nu/aN^{1/2}$ [see Fig. 2; recall that $S_N(\mathbf{k})$ is cylindrically symmetric about the $\hat{\mathbf{n}}$ axis and note that when $\nu\to 0$, $|\mathbf{k}|$ is approximately equal to the radial component of $\mathbf{k}$ over most of the plot]. The broad peaks imply that smectic-C type fluctuations become virtually degenerate with the smectic-A ones up to very large tilt angles, which allows us to invoke the Brazovskii argument. Thus, the nematic/smectic-A transition could also be driven discontinuous by fluctuations provided that ν is sufficiently small. Note that as with conventional coil-coil diblocks, the Brazovskii fluctuations are suppressed by an increase in molecular weight.[4]

Our exact mean-field results can be compared[19] with the analytical approximations used in Refs. 7–9. It is evident from the phase diagram in Ref. 8 that these approximations are quantitatively inaccurate at the degrees of segregation in our study. Furthermore, they are not qualitatively correct in all regards. For instance, a large portion of the smectic-A/smectic-C boundary is predicted to be discontinuous. Also the boundaries separating the smectic-A monolayer and bilayer phases are at odds with our calculations; at small f, Ref. 8 predicts the boundary to be discontinuous, and at larger f, they predict that the smectic-C bilayer phase will completely separate the two smectic-A phases. Nevertheless, the analytical approximations do provide a reasonable description of the phase behavior and they are valuable for developing intuitive explanations.

Recently, Chen *et al.*[10,11] have synthesized five diblock copolymers by joining a rigid polyhexyl-isocyanate (PHIC) block with a flexible polystrene (PS) block. The characteristics of these molecules are listed in Table I along with a description of their respective morphologies. They all have large rod fractions and thus should be well represented by the present model. Indeed, each sample produced a smectic lamellar-type phase. Because the rods crystallized, the tilt angle was restricted to $\theta=0.0°, 45.9°, 64.2°, 72.1°, \ldots$,[10] but still the expected trend in tilt angle was evident. In particular, the largest coil fraction $f=0.58$ produced a monolayer smectic-C phase with the greatest tilt angle, $\theta\approx 60°$. Because this sample exhibited poor long-range order, it was termed the ''wavy'' lamellar phase. The intermediate coil fractions produced a bilayer smectic-C phase with a lower tilt angle, and because of a large population of kink grain boundaries (see Fig. 9),[20] this phase was labeled as the ''zig-zag'' morphology. At the lowest coil fractions, an unusual smectic-O phase occurred, where the tilt angle of the rods flipped from layer to layer, producing what was called the ''arrowhead'' morphology.

Although the general behavior in Refs. 10 and 11 is consistent with our predictions, a number of features are not captured by our calculation. However, we suspect these are a

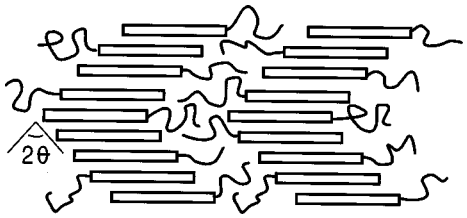

FIG. 9. Schematic diagram of a low-energy 2θ kink boundary in a smectic-C lamellar phase.

consequence of nonequilibrium effects associated with the solvent-casting process. Indeed, Ref. 10 reported that morphology depends significantly on the particular solvent used to prepare samples. The process of solvent casting first disorders the rod-coil molecules by diluting them with a solvent. As the solvent slowly evaporates, the rod concentration increases and a nematic phase forms with hopefully long-range order. Further evaporation increases the unfavorable contacts between the coil and rod segments eventually producing a smectic phase. We suspect that the zig-zag samples became smectic-C at this point, while the arrowhead samples produced a smectic-A structure. As more solvent evaporated, the tilt angle in the zig-zag morphology must have varied up to the point where crystallization occurred. The changing tilt angle could easily induce a large number of low-energy kink boundaries like those depicted in Fig. 9. We suspect that the arrowhead morphology occurred due to a smectic-A/smectic-C transition. So as to cause a minimal deformation of the sample, the tilting rods may have folded up like an accordion to produce a smectic-O structure. In such a structure, kink boundaries would be very costly, and hence the smectic-O phase should exhibit long-range lamellar order. The occurrence of bilayer phases can also be attributed to the solvent, because it reduces the steric interactions. Although a bilayer phase might become unstable as the last bit of solvent evaporates, ultraslow kinetics at that point would almost certainly prevent it from converting to a more stable monolayer phase. Thus, the bilayers, the kink boundaries in the zig-zag morphology, and the smectic-O character of the arrowhead morphology may all be related to the solvent-casting process, rather than to the equilibrium behavior.

VIII. SUMMARY

We have examined the phase behavior of the Semenov–Vasilenko model[7] for rod-coil diblock copolymers. Our results are presented in terms of the conventional diblock copolymer parameters:[19] χN for the degree of segregation and f for the volume fraction of the coil block. It is also necessary to specify the ratio $\nu = aN^{1/2}/bN$ of the two length scales, $aN^{1/2}$ and bN, corresponding to the coils and rods, respectively. By applying self-consistent field techniques,[14] we have eliminated the approximations used in previous studies[7–9] to generate the exact mean-field phase diagram in Fig. 8. Fluctuation effects are still ignored, but they should be negligible except perhaps near the nematic/smectic boundary, where they can create a discontinuity in the transitions. The steric effects of the rods impart fairly classical liquid-crystalline behavior onto this system. The molecules exhibit a nematic (N) phase at high-temperatures where the rods and coils mix, and they display smectic lamellar phases once the rod and coils microphase separate. At high coil fractions ($f \gtrsim 0.7$), the model should also exhibit nonlamellar structures,[6,9,12] but we have not included them in our study. The typical lamellar phase displays the smectic-C (S_C) structure shown in Fig. 1(a), where tilted rods form monolayer domains. The tilt angle θ is, in general, controlled by a competition between interfacial tension and coil stretching, which favor low and high tilt angles, respectively. Toward small f where the coil stretching is reduced, $\theta \to 0$ producing a continuous transition to a monolayer smectic-A phase. Beyond that, the high interfacial energy favors the formation of a bilayer phase like that shown in Fig. 1(b), but this is strongly opposed by the steric interactions. For small coils or very weak degrees of segregation, a smectic-A regime exists with a significant population of rods penetrating deep into the coil domains producing a neutral state where the coils are virtually unstretched.

Of the molecules synthesized so far, the ones that best represent the present model are the five polyhexylisocyanate/polystrene (PHIC/PS) diblock copolymer samples created by Chen *et al.*[10,11] (see Table I). The PHIC block has a long persistent length of ~ 550 Å, while the PS block is highly flexible. Each sample produced a smectic lamellar morphology as expected given their large rod volume fractions. Although the PHIC blocks crystallized quantizing the tilt angle in most cases to $\theta = 45°$, the sample with the largest coil fraction did exhibit a larger θ supporting our predicted trend. However, the experiments also observed a number of interesting features not anticipated by the theory, but we attribute these to nonequilibrium effects associated with the solvent-casting procedure used to prepare the samples. Their zig-zag morphology could have resulted from low-energy kink boundaries produced as the tilt angle changed during solvent evaporation, and their smectic-O arrowhead morphology may have occurred because of a smectic-A/smectic-C transition during the solvent evaporation. We also attribute the prevalence of bilayer structures to the solvent, because of its ability to reduce the steric interactions.

Theory and experiment have sketched out a reasonably consistent picture of rod-coil diblock copolymer phase behavior, but there are still many issues to be resolved. On the experimental side, this will require synthesizing more molecules, and carefully distinguishing nonequilibrium effects from the equilibrium behavior. This will best be done by working in the weak- to intermediate-segregation regime, where nonequilibrium effects are hopefully not too severe. Certainly there is much to learn about solvent effects. We are currently pursuing calculations to address our suggestion that small concentrations of solvent have dramatic effects on the phase behavior. It would also be nice to have calculations that more accurately examine the nonlamellar phases at large f by extending our self-consistent field technique. Once this is accomplished, we will be well prepared to tackle more complicated liquid-crystalline block copolymer architectures from which we can anticipate an even richer selection of interesting phenomena.

ACKNOWLEDGMENT

We thank E. L. Thomas for supplying us with details regarding the experiments in Refs. 10 and 11.

APPENDIX

Here we calculate the structure function, $S_N(k,\theta)$, by expanding the free energy about the nematic state. First the fields are approximated by $w(z)\approx w_1\sqrt{2}\cos(kz)$ and $u(z)\approx u_1\sqrt{2}\cos(kz)$. The initial condition for $q^\dagger(z,s)$ is straightforward to evaluate,

$$q^\dagger(z,f)\approx(2+u_1^2)-2u_1\cos(kL_z)\sqrt{2}\cos(kz). \tag{A1}$$

By writing $q(z,s)\approx q_0(s)+q_1(s)\sqrt{2}\cos(kz)$ and using Eq. (13), we obtain the relations

$$\frac{d}{ds}q_0(s)\approx -w_1q_1(s), \tag{A2}$$

$$\frac{d}{ds}q_1(s)\approx -w_1q_0(s)-k^2a^2Nq_1(s)/6, \tag{A3}$$

where $q_0(0)=1$ and $q_1(0)=0$. Next, we solve Eq. (A3) for $q_1(s)$ using the approximation $q_0(s)\approx 1$, and then we solve Eq. (A2) to improve the approximation for $q_0(s)$. This provides us with

$$q(z,s)\approx 1+w_1^2g(s,k^2a^2N/6) - w_1h(s,k^2a^2N/6)\sqrt{2}\cos(kz), \tag{A4}$$

where $g(s,x)\equiv(\exp(-xs)-1+xs)/x^2$ and $h(s,x)=(1-\exp(-xs))/x$. With that we can evaluate $\mathcal{Q}$ to quadratic order in the fields:

$$\mathcal{Q}/\mathcal{S}\approx 2+S_{11}w_1^2+2S_{12}\gamma^{-1}w_1u_1+S_{22}\gamma^{-2}u_1^2, \tag{A5}$$

where γ and S_{ij} are defined in Sec. III. Then from the definition of the densities, Eqs. (17) and (18), we obtain

$$\phi_{C,1}=-S_{11}w_1-S_{12}\gamma^{-1}u_1, \tag{A6}$$

$$p_{R,1}=-S_{12}\gamma^{-1}w_1-S_{22}\gamma^{-2}u_1. \tag{A7}$$

Inverting these equations provides expressions for the fields:

$$w_1=(S_{12}\gamma p_{R,1}-S_{22}\phi_{C,1})/(S_{11}S_{22}-S_{12}^2), \tag{A8}$$

$$u_1=\gamma(S_{12}\phi_{C,1}-S_{11}\gamma p_{R,1})/(S_{11}S_{22}-S_{12}^2). \tag{A9}$$

Furthermore, Eqs. (6) and (9) provide the relations,

$$\phi_{R,1}=\gamma p_{R,1}=-\phi_{C,1}. \tag{A10}$$

Now we have all the quantities necessary to evaluate the free energy, Eq. (5), to second order in $\phi_{C,1}$. With simple substitutions and the approximation, $\ln(2+x)\approx\ln(2)+x/2-x^2/8$, we arrive at

$$\frac{F}{nk_BT}\approx -\ln(2)-\frac{1}{2}S_{11}w_1^2-S_{12}\gamma^{-1}w_1u_1-\frac{1}{2}S_{22}\gamma^{-2}u_1^2 + \chi N[f(1-f)+\phi_{C,1}\phi_{R_1}]-w_{C,1}\phi_{C,1} - u_{R,1}p_{R,1}-\ln(f)+\frac{\cos(kL_z)}{f}p_{R,1}\phi_{R,1} + \frac{1}{2f^2}\phi_{R,1}^2. \tag{A11}$$

Substituting Eqs. (A8)–(A10) into Eq. (A11) and comparing with Eq. (24) immediately yields the expression in Eq. (25) for $S_N(k,\theta)$.

[1] F. S. Bates and G. H. Fredrickson, Annu. Rev. Phys. Chem. **41**, 525 (1990).
[2] P. M. Duessing, R. H. Templer, and J. M. Seddon, Langmuir **13**, 351 (1997).
[3] M. W. Matsen and F. S. Bates, Macromolecules **29**, 7641 (1996); J. Chem. Phys. **106**, 2436 (1997).
[4] G. H. Fredrickson and E. Helfand, J. Chem. Phys. **87**, 697 (1987); I. W. Hamley and V. E. Podneks, Macromolecules **30**, 3701 (1997).
[5] M. W. Matsen and F. S. Bates, Macromolecules **29**, 1091 (1996).
[6] S. I. Stupp, Curr. Opin. Colloid Interface Sci. **3**, 20 (1998).
[7] A. N. Semenov and S. V. Vasilenko, Sov. Phys. JETP **63**, 70 (1986).
[8] A. N. Semenov, Mol. Cryst. Liq. Cryst. **209**, 191 (1991).
[9] D. R. M. Williams and G. H. Fredrickson, Macromolecules **25**, 3561 (1992).
[10] J. T. Chen, E. L. Thomas, C. K. Ober, and G.-P. Mao, Macromolecules **28**, 1688 (1995).
[11] J. T. Chen, E. L. Thomas, C. K. Ober, and G.-P. Mao, Science **273**, 343 (1996).
[12] L. H. Radzilowski and S. I. Stupp, Macromolecules **27**, 7747 (1994); L. H. Radzilowski, B. O. Carragher, and S. I. Stupp, *ibid.* **30**, 2110 (1997).
[13] E. Helfand, J. Chem. Phys. **62**, 999 (1975).
[14] M. W. Matsen and M. Schick, Phys. Rev. Lett. **72**, 2660 (1994).
[15] M. Müller and M. Schick, Macromolecules **29**, 8900 (1996).
[16] R. Hołyst and M. Schick, Macromolecules **96**, 730 (1992); D. R. M. Williams and A. Halperin, Phys. Rev. Lett. **71**, 1557 (1993); C. Singh, M. Goulian, A. J. Liu, and G. H. Fredrickson, Macromolecules **27**, 2974 (1994); R. R. Netz and M. Schick, Phys. Rev. Lett. **77**, 302 (1996).
[17] A. Halperin, Europhys. Lett. **10**, 547 (1989); Macromolecules **23**, 2724 (1990).
[18] S. A. Brazovskii, Sov. Phys. JETP **41**, 85 (1975).
[19] The parameters used in Refs. 7–9 are related to the present ones by the expressions: $\chi_s=(1-f)\chi N$, $\lambda_s=f/(1-f)$, $\nu_s=\nu^2/6(1-f)$, $v_s=\rho_0^{-1}$, $N_s=fN$, $a_s=a/6^{1/2}$, $L_s=(1-f)bN$, and $d_s=(\rho_0 b)^{-1/2}$, where the subscript, s, denotes the parameters defined by Semenov and Vasilenko.
[20] S. P. Gido and E. L. Thomas, Macromolecules **27**, 6137 (1994); M. W. Matsen, J. Chem. Phys. **107**, 8110 (1997).